Remote Sens. **2014**, *6*, 5090-5106; doi:10.3390/rs6065090

OPEN ACCESS

remote sensing

ISSN 2072-4292

www.mdpi.com/journal/remotesensing

Article

A Spectral Decomposition Algorithm for Estimating Chlorophyll-*a* Concentrations in Lake Taihu, China

Yuchao Zhang [1,†], Ronghua Ma [1,*], Hongtao Duan [1,†], Steven Loiselle [2,†] and Jinduo Xu [1,†]

[1] State Key Laboratory of Lake Science and Environment, Nanjing Institute of Geography and Limnology, Chinese Academy of Sciences, Nanjing 210008, China;
E-Mails: yczhang@niglas.ac.cn (Y.Z.); htduan@niglas.ac.cn (H.D.); jdxu@niglas.ac.cn (J.X.)

[2] Department of Biotechnology, Chemistry and Pharmacy, University of Siena, CSGI, Via Aldo Moro 2, Siena 53100, Italy; E-Mail: loiselle@unisi.it

† These authors contributed equally to this work.

***** Author to whom correspondence should be addressed; E-Mail: rhma@niglas.ac.cn; Tel.: +86-25-8688-2168; Fax: +86-25-5771-4759.

Received: 28 March 2014; in revised form: 31 March 2014 / Accepted: 23 May 2014 / Published: 5 June 2014

Abstract: The complex interactions among optically active substances in Case II waters make it difficult to associate the variability in spectral radiance (or reflectance) to any single component. In the present study, we developed a four end-member spectral decomposition model to estimate chlorophyll-*a* concentrations in a eutrophic shallow lake—Lake Taihu. The new model was constructed by simulated spectral data from Hydrolight and was successfully validated using both of simulated reflectance and *in situ* reflectance data. Using MEdium Resolution Imaging Spectrometer (MERIS) images, the accuracy of the new model was estimated and compared with other published models. According to the MERIS retrieved results, the spatial distribution of chlorophyll-*a* concentrations and its relationship with environment factors were analyzed. The application of the new model and its limits to estimate water surface chlorophyll-*a* concentrations in turbid lakes is also discussed.

Keywords: spectral decomposition algorithm; chlorophyll-*a*; Case II waters; Lake Taihu

---

1. Introduction

Phytoplankton biomass is one of the three main components influencing the optical properties of natural waters. The concentration of chlorophyll-*a* (Chla, $\mu g \cdot L^{-1}$) has been used as a marker for phytoplankton biomass and in calculations of bio-production of many waters [1]. According to the bipartite classification scheme [2–4], oceanic (or fresh) waters are classified into one of two types: Case I or Case II. Case I waters are considered to encompass over 90% of the world oceans, and Case II waters include many coastal and inland waters of which economic, social, and ecological significance is significant. Phytoplankton biomass is the principal agent responsible for variations in the optical properties of Case I waters. Case II waters are influenced, not only by phytoplankton and related particles, but also by other optically active substances that vary independently of phytoplankton, notably suspended inorganic particles and dissolved organic matter [5]. Thus, it is generally recognized that Case II waters are more complex than Case I waters in their composition and optical properties. Case I waters can be typically treated as a single-variable problem, while Case II waters must be addressed in a non-linear, multivariate manner [5]. As a result, the application of algorithms from Case I waters (such as the ratio of the near-infrared (NIR) peak reflectance to the reflectance near 675 nm, fluorescence line height and first derivative of reflectance algorithm) does not provide acceptable results for Case II waters [6–8]. In general, the estimation of Chla in Case II waters requires more than simple adjustments to the Case I algorithms.

In recent studies, a three-band semi-analytical algorithm has been successfully used to assess Chla distributions in turbid waters without re-parameterization [8–10]. However, the assumptions for the three-band semi-analytical algorithm may be violated in highly turbid waters, as particle absorption and backscattering vary with the type of suspended particles [11,12]. Four-band semi-analytical algorithms and enhanced three-band semi-analytical algorithms provide robust alternatives [12–14], but require further development.

In terrestrial studies, the consideration of a given pixel as a linear combination of individual components has been widely applied. This approach has also been used in aquatic studies [15–17]. According to this model, the observed reflectance spectra can be disaggregated into the sum of the spectra of several optically active components. Each spectrum is weighted by the relative proportion of each optically active component. In general, this is achieved by: identifying optically active components (end-members) and their spectra; constructing the relationship between decomposition coefficients and corresponding optically active components. Svab [18], Novo [19], Tyler [17] and Oyama [20–22] measured the reflectance spectra of end-members by laboratory determination. Others used satellite image-derived reflectance spectra of end-members [23–25]. However, in the former case, the reflection from interior walls of the mesocosm (or tank) was found to influence the accuracy of the end-members' spectra. In the latter case, differences in the signal to noise and atmospheric correction processes for different images were found to reduce the accuracy of end-members' spectra [26]. Pilorz and Davis (1990) suggested the use of libraries of absorption and scattering coefficients to model upwelling reflectance [27]. Radiative transfer numerical models, such as HYDROLIGHT, estimate spectral radiance distributions, based on the absorbing and scattering properties of the water body, the sky radiance incident onto the water surface, the wind speed, and the bottom

reflectance [28,29]. These models help to simulate reflectance under different environment conditions, especially extreme conditions.

Based on spectrally unique end-members, Svab [18] and Tyle [17] used principal component analysis (PCA) to characterize the spectra of shallow lakes, and combined multivariate regression and a spectral linear mixture modeling approach to retrieve Chla. Oyama [20–22] developed the spectral decomposition algorithm (SDA) to estimate Chla in Lake Kasumigaura of Japan, which considered the mixed reflectance spectrum of a given pixel as a linear combination of three dominant components (water, non-phytoplankton suspended sediment (NPSS), and phytoplankton). However, the use of these methods in other water bodies, in particular in the hyper-eutrophic and spatially heterogeneous inland water bodies where dissolved organic matter contribute to overall optical conditions has not been explored.

Lake Taihu, based on the *in situ* measurements during the period of 2008–2011, was found to have a seasonal and spatial distribution of dominant optical components. The absorption of non-pigment containing particles and colored dissolved organic matter absorption was found to dominate in autumn, while the absorption of phytoplankton pigment, non-pigment containing particles, and colored dissolved organic matter (CDOM) was most important in the summer [30].

Considering the optical challenges of these waters, the present study used data from Lake Taihu (China) to focus on: (1) simulating the spectra of end-members of the dominant optical components in this eutrophic shallow lake; (2) developing a four end-members spectral decomposition model (water, NPSS, phytoplankton, and CDOM); (3) validating the developed model with *in situ* data and MERIS data; (4) analyzing the Chla distribution and its environmental impact, and discussing the application and limits of the new model in eutrophic and turbid lakes.

2. Study Area

Lake Taihu is located in the center of China's Yangtze River Delta (Figure 1). With a surface area of 2428 km^2 and an average depth of 2 m (maximum depth of 3 m) [31], it is the third largest lake in China after Lake Poyang and Lake Dongting. With the recent rapid economic development of the region, Lake Taihu has become eutrophic with more frequent and more severe cyanobacteria blooms [31–33]. In recent decades, algal bloom events have jeopardized the supply of drinking water to millions of people in the surrounding cities [34,35].

Studies show Chla ranging from 0.13 to 148.3 $\mu g \cdot L^{-1}$ and cyanobacteria (*Microcystis*) dominated the phytoplankton community composition throughout the year [36]. Total suspended sediment (TSS) concentrations ranged from 7.8 to 169.5 $mg \cdot L^{-1}$, due mainly to the resuspension of bottom sediments [37]. The concentration of dissolved organic carbon (DOC) reached 17.2 $mg \cdot L^{-1}$ [38] with the corresponding CDOM (Chromophoric dissolved organic matter) absorption coefficient at 420 nm ranging from 0.5 to 4.8 m^{-1}. This latter is significantly higher than CDOM absorption observed by Oyama *et al*. [21], in Lake Kasumigaura (0.5–0.6 m^{-1}).

Figure 1. Lake Taihu, China in the Yangtze River Delta. The lake is divided into lake sections, including Zhushan Bay (ZB), Meiliang Bay (MB), Gong Bay (GB), West Lake (WL), South Lake (SL), Central Lake (CL), East Lake, and East Taihu.

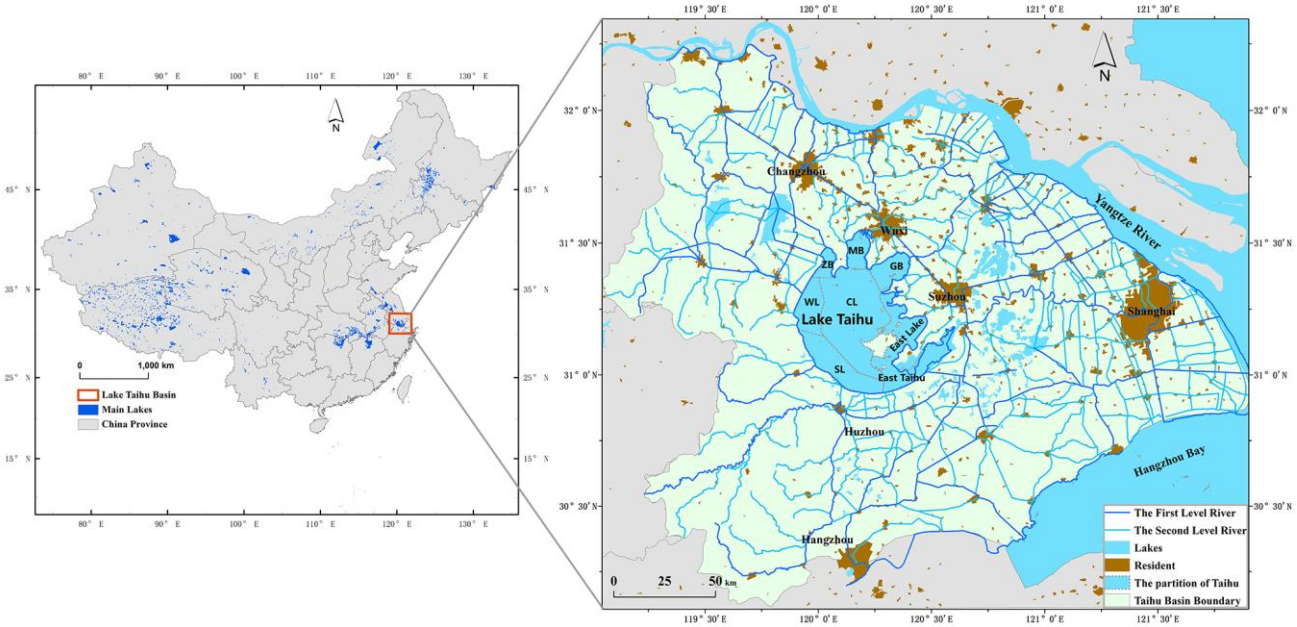

3. Materials

3.1. Simulated Dataset

A simulated dataset was generated using the Hydrolight radiative transfer model [28]. This dataset consisted of: the end-member simulated spectra of the concentration of each single end-member (*i.e.*, NPSS, phytoplankton, CDOM, water), the model-construction dataset and the model-validation dataset. The latter two datasets include 248 combinations of these end-members, which were divided randomly into a construction dataset (204 combinations) and a validation dataset (44 combinations).

The input parameters for the radiative transfer model were:

- Inherent optical property (IOP) specification model: CASE2;
- Pure water IOP [39];
- IOP specifications for Chla, NPSS and CDOM including a concentration profile, specific absorption and specific scattering spectra [26];
- Internal Source and Inelastic Scatter Selection linked to Chlorophyll Fluorescence, CDOM Fluorescence and Raman Scattering;
- Wind speed of 3.5 m/s (average of wind speed in Lake Taihu) and solar zenith angle of 30 °;
- Parameters of air-water surface boundary conditions, sky conditions and bottom boundary condition were set to their default values.

3.2. Field Measurements

Two data collection campaigns (60 samples) were performed in March and September 2011 in Lake Taihu (Table 1 and Figure 2). At each station, water samples were collected from the surface to a

depth of 30 cm for measurement in the laboratory and GPS coordinates (0.3–3 m accuracy) were recorded. Chla was determined by the standard spectrophotometric methods following extraction using 90% ethanol [12]. Above-surface remote sensing reflectance spectra between 350 and 1050 nm (1 nm resolution) were measured with a FieldSpec Pro Dual VNIR (ASD, USA) following NASA protocols [40]. Field measurements were performed from 09:30 to 14:30 local time in sunny conditions with low wind speed (<3.5 m/s). The Chla data and water surface reflectance were used to validate the new model.

Another four data collection campaigns (52 samples) were performed in April 2008 October 2008 (two campaigns) and May 2011 (Table 1 and Figure 2). Only water samples with GPS coordinates and coincident MERIS images were used to analyze the Chla distribution.

Table 1. Chla ($\mu g \cdot L^{-1}$) in Lake Taihu (SD: standard deviation; CV: coefficient of variation in percent (*i.e.*, SD/mean of parameter)).

Data Type	Numbers	Minimum	Maximum	Mean	SD	CV
27 March 2011	33	5.45	31.05	16.82	6.53	0.39
3 September 2011	27	13.13	160.93	49.78	38.90	0.78
24 April 2008	11	7.76	58.5	26.53	18.90	0.71
13 October 2008	8	4.16	14.81	9.86	3.63	0.37
16 October 2008	21	10.86	43.56	20.86	7.92	0.38
1 May 2011	12	5.28	37.06	18.36	10.24	0.56

Figure 2. Distribution of sample stations in Lake Taihu.

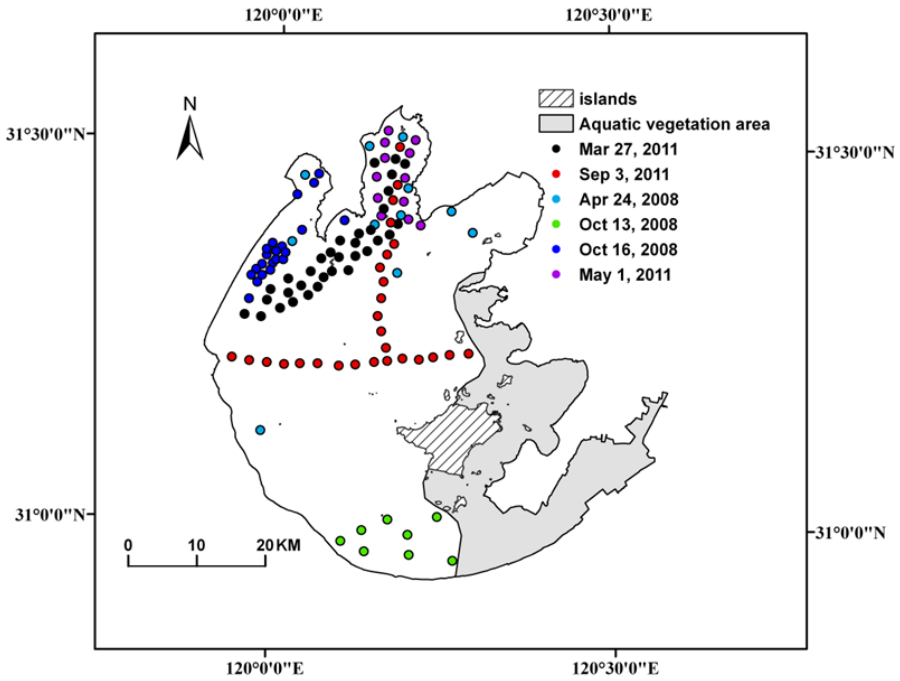

3.3. MERIS Images

Four Medium Resolution Imaging Spectrometer (MERIS) FR images were used to coincide with field campaigns on 24 April, 13 October, and 16 October 2008 and 1 May 2011. MERIS data have a

spatial resolution (300 × 300 m at nadir) and spectral properties (15 narrow bands in the visible and near-infrared) that is appropriate for the optical analysis of larger inland waters [41–44]. Frequent cloud cover over Lake Taihu prevented more match-ups between satellite overpasses and the field measurements. The time span between field and the MERIS observation was approximately 2 h, short enough for comparison of the spectral reflectance measurements. The atmospheric correction algorithms were based on the Basic ERS and ENVISAT (A)ATSR and MERIS Toolbox (BEAM) with the Lake/Eutrophic option [45].

4. Methods

4.1. The Spectral Decomposition Algorithm for Lake Taihu

Lake Taihu is characterized by an elevated CDOM. Accordingly, water, phytoplankton biomass, NPSS and CDOM were included as end members in the new algorithm. The spectral decomposition algorithm for Lake Taihu considered the mixed reflectance spectra $R(\lambda)$ as a linear combination (Equation (1)):

$$R(\lambda) = C_p \times R_p(\lambda) + C_n \times R_n(\lambda) + C_c \times R_c(\lambda) + C_w \times R_w(\lambda) \quad (1)$$

where C_p, C_n, C_c, and C_w are the decomposition coefficients of phytoplankton, NPSS, CDOM and water, respectively, directly related to their relative masses (e.g., concentrations). $R_p(\lambda)$, $R_n(\lambda)$, $R_c(\lambda)$, and $R_w(\lambda)$ are the standard reflectance spectra for each component [20,21]. Four decomposition coefficients were calculated (*i.e.*, C_p, C_n, C_c, and C_w) by selecting four MERIS bands (Equation (2)).

$$\begin{aligned} R(\lambda_1) &= C_p \times R_p(\lambda_1) + C_n \times R_n(\lambda_1) + C_c \times R_c(\lambda_1) + C_w \times R_w(\lambda_1) \\ R(\lambda_2) &= C_p \times R_p(\lambda_2) + C_n \times R_n(\lambda_2) + C_c \times R_c(\lambda_2) + C_w \times R_w(\lambda_2) \\ R(\lambda_3) &= C_p \times R_p(\lambda_3) + C_n \times R_n(\lambda_3) + C_c \times R_c(\lambda_3) + C_w \times R_w(\lambda_3) \\ R(\lambda_4) &= C_p \times R_p(\lambda_4) + C_n \times R_n(\lambda_4) + C_c \times R_c(\lambda_4) + C_w \times R_w(\lambda_4) \end{aligned} \quad (2)$$

Each decomposition coefficient C_p was then used as an independent variable in the Chla retrieval model. The algorithm had two component parts based on: information about the individual masses of the optically active components and information about spectral properties. Therefore, the estimation model of Chla can be expressed by Equation (3):

$$C_{Chla} = f(C_p) \quad (3)$$

where C_{Chla} and C_p are the decomposition coefficients for Chla and phytoplankton respectively. As there are many functional expressions between C_{Chla} and C_p, the final expression was determined by the regression analysis.

4.2. The Spectral Properties of End-Members

An end member's standard spectra should include only the spectral information of the end member without the influence of the other end members. As it is very difficult to achieve these spectra by field-measured reflectance in the lake, two approaches have been used in the past: lab-experiment and the radiative transfer modeling. For the former, recent studies indicate that reflectance from tank walls and bottom can compromise the determination of individual spectra [20]. Another difficulty is related

to the separation of CDOM from the lake water without modification of its optical properties. Ideally, a radiative transfer model is preferable in the determination of the standard spectra of each end member.

The link between reflectance and end-member concentration at each wavelength was based on the simulated spectra of each end-member (NPSS, phytoplankton, CDOM, and water). For each end member, an increase in concentration brings the reflectance spectra closer to saturation, and accordingly, the reflectance differentiation would decrease. We used the ratio of reflectance differentiation to maximum reflectance differentiation of each end-member (Equation (4)) to determine the concentration and the standard reflectance spectrum.

$$Ratio = D(\lambda)/D_{max} \quad (4)$$

where $D(\lambda)$ and D_{max} was defined as $dR(c,\lambda)/dc$ and *maximum of* $D(\lambda)$, respectively; λ was the wavelength of the reflectance spectra; c was the concentration (or absorption) of phytoplankton, NPSS, or CDOM.

When the phytoplankton reflectance ratio was lower than 3%, slight variations in the spectra were found. Reflectance ratio thresholds of NPSS and CDOM for the standard spectra were determined in the same way. For the present study, the ratios of 3%, 2%, and 1% were used for phytoplankton, NPSS and CDOM standard spectra (Figure 3), corresponding concentrations (or absorption) of 150 $\mu g \cdot L^{-1}$, 100 $mg \cdot L^{-1}$, and 3.5 m^{-1}, respectively. These results support those reported by Lu [26].

Figure 3. The standard spectra of end-members (water, Chla, NPSS, and CDOM) for concentrations (or absorption) of 150 $\mu g \cdot L^{-1}$, 100 $mg \cdot L^{-1}$, and 3.5 m^{-1}, respectively.

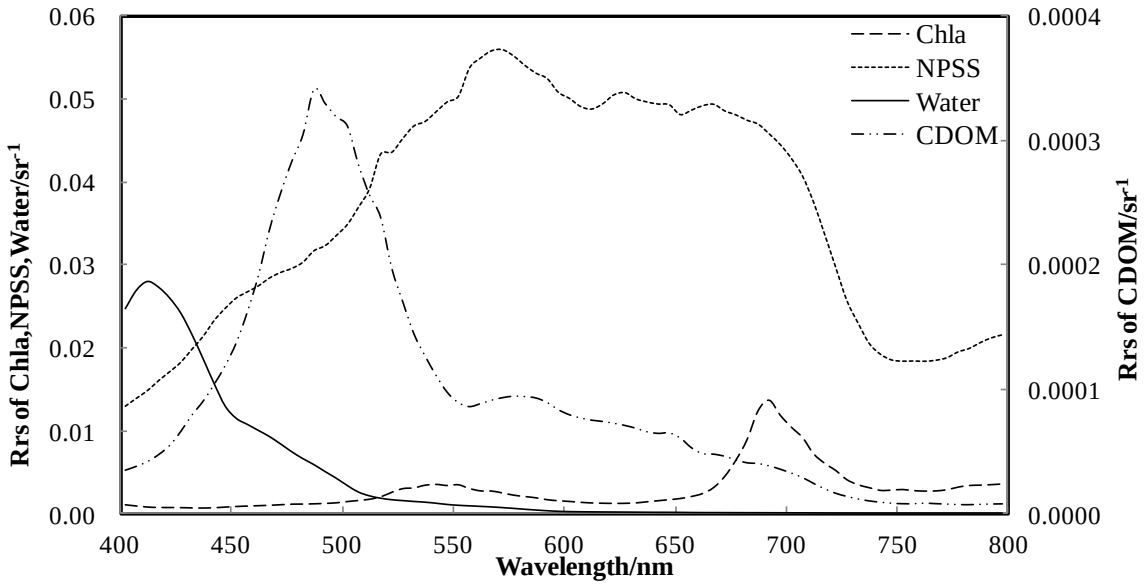

5. Results

The mixed reflectance and standard reflectance at the same wavelength could complete one of the four equations. Four equations (Equation (2)) at four different wavelengths were used to determine C_p, C_n, C_c, and C_w. The MERIS bands considered most sensitive to Chla were tested with the simulated data set (n = 204) (Table 2). Model M7, including MERIS bands 3 (490 nm), 5 (560 nm), 8 (681.25 nm), and 9 (708.75 nm), provided the best correlation (R^2 = 0.82, Figure 4) with Chla. For Case II waters,

low reflectance at wavelengths less than 500 nm has been associated to absorption by both algal pigments (e.g., Chla) and dissolved organic matter [46]. Likewise, an increase in reflectance at wavelengths 510–620 nm has been associated to low absorption by phytoplankton pigments coupled with increased backscattering due to high particle concentration [47]. A peak of reflectance at 685–715 nm was due to chlorophyll-*a* fluorescence [48].

The relationship between the decomposition coefficient and Chla was determined by regression analysis as (Equation (5) and Figure 4):

$$C_{Chla} = 18.219 \times e^{1.149Cp} \quad (5)$$

Table 2. Accuracy evaluation of different spectral decomposition models using MERIS band-combinations of the simulated model-construction dataset.

Models	MERIS Bands	Function with C_p	R^2	RE (%)	RMSE (μg·L^{-1})
M1	2,5,7,9	$y = 8.7261C_p^2 - 3.4274C_p + 15.119$	0.6147	46.50	30.40
M2	2,5,7,10	$y = 0.1353C_p^2 - 13.153C_p + 19.107$	0.5750	51.29	32.04
M3	2,5,8,9	$y = 0.0204C_p^2 + 0.884C_p + 26.684$	0.5246	62.91	33.89
M4	2,5,8,10	$y = 0.44C_p^2 - 10.25C_p + 41.46$	0.4813	137.15	35.39
M5	3,5,7,9	$y = 19.214e^{0.856Cp}$	0.7722	33.58	20.62
M6	3,5,7,10	$y = 1.8896C_p^2 - 18.66C_p + 56.518$	0.7449	54.54	24.82
M7	3,5,8,9	$y = 18.219e^{1.1498Cp}$	0.8169	30.10	18.55
M8	3,5,8,10	$y = 42.903e^{1.2412Cp}$	0.5552	52.78	33.00

Figure 4. The relationship between the decomposition coefficients of phytoplankton (C_p) and Chla based on Hydrolight simulated data.

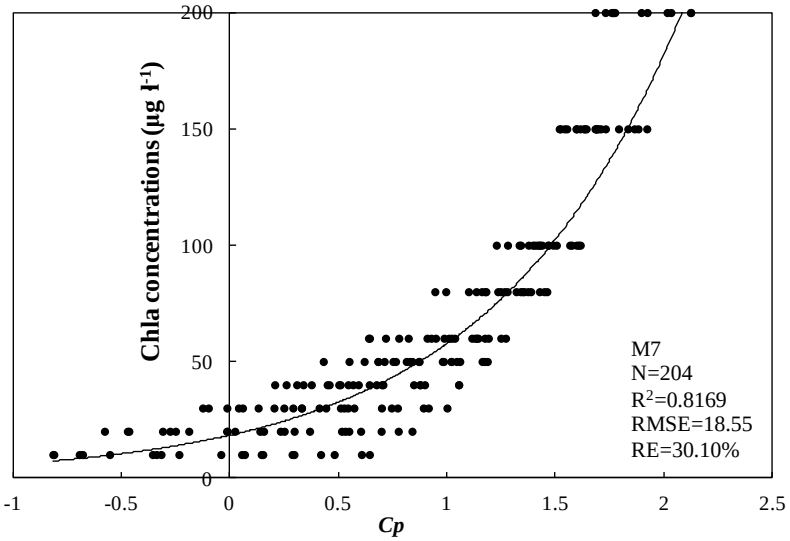

6. Validation

The RMSE (Root Mean Square Error) and RE (Relative Error) between measured and retrieved values were calculated as:

$$RMSE = \sqrt{\frac{\sum(C_m - C_r)^2}{N - 1}} \quad (6)$$

$$RE = \frac{1}{N}\sum \frac{ABS(C_m - C_r)}{C_m} \quad (7)$$

where C_m and C_r are the measured and retrieved Chla, respectively, and N is the number of data points.

The model-validation dataset of 44 combinations of the end-members showed that the performance of the model was good, with *RMSE* 15.9 μg·L^{-1} and *RE* 34.4% (Figure 5).

Figure 5. The comparison of *in situ* Chla and retrieved Chla using the spectral decomposition model.

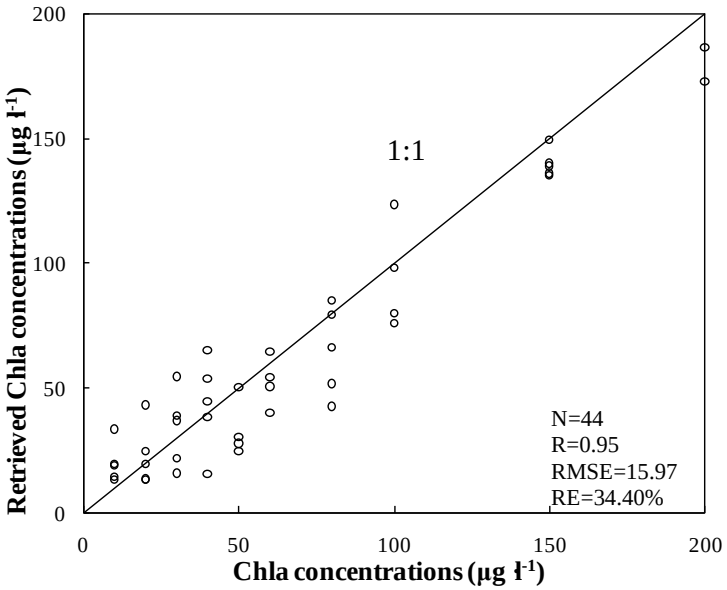

We then used the model and the *in situ* water surface reflectance in March and September of 2011 to estimate Chla, which were below 100 μg·L^{-1} (Table 3). The new model showed good results in retrieving Chla, with a total *RMSE* of 7.50 μg·L^{-1} and a *RE* of 30.4%. Two samples in the range of 40–50 μg·L^{-1} had unusually high *RMSE* and *RE*.

Table 3. Validation of the spectral decomposition model with *in situ* data.

Range	Samples	RMSE (μg·L^{-1})	RE (%)
0 < Chla ≤ 10 μg·L^{-1}	4	6.04	86.89
10 < Chla ≤ 20 μg·L^{-1}	27	5.82	31.85
20 < Chla ≤ 30 μg·L^{-1}	10	8.22	28.22
30 < Chla ≤ 40 μg·L^{-1}	7	9.58	23.46
40 < Chla ≤ 50 μg·L^{-1}	2	20.76	47.98
50 μg·L^{-1} < Chla	10	7.98	7.57

7. Discussions

7.1. Accuracy Estimation Using MERIS Data

To further assess the accuracies of the algorithms, data from the 52 stations (Table 1, Figure 2) were collected on the same day as MERIS image acquisition. Our new model was compared to six models

developed by Li [14], a model by Moses [49], a model by Mishra [50], and a model by Zhou [51] (Table 4). The new model provided a similar *RE* with respect to the other models and a smaller *RMSE*.

Table 4. Comparison of nine models with MERIS data.

Model	Bands Combination	RMSE (μg L^{-1})	RE (%)
LI-1 model	$(R_{rs}^{-1}(b7) - R_{rs}^{-1}(b9))R_{rs}(b10)$	12.76	55.71
LI-2 model	$(R_{rs}^{-1}(b7) - R_{rs}^{-1}(b9))/(R_{rs}^{-1}(b10) - R_{rs}^{-1}(b9))$	16.41	61.62
LI-3 model	$(R_{rs}^{-1}(b8) - R_{rs}^{-1}(b9))R_{rs}(b10)$	10.56	51.62
LI-4 model	$(R_{rs}^{-1}(b8) - R_{rs}^{-1}(b9))/(R_{rs}^{-1}(b10) - R_{rs}^{-1}(b9))$	10.01	53.82
LI-5/Moses' model	$R_{rs}(b9)/R_{rs}(b7)$	13.59	60.56
LI-6 model	$R_{rs}(b9)/R_{rs}(b8)$	14.78	53.00
Zhou's model	$(R_{rs}^{-1}(b8) - R_{rs}^{-1}(b9))/(R_{rs}^{-1}(b10) - R_{rs}^{-1}(b9))$	8.75	64.56
Mishra's model	$(R_{rs}(b9) - R_{rs}(b7))/(R_{rs}(b9) + R_{rs}(b7))$	10.98	54.64
New model	M7(band 3,5,8,9)	8.45	58.06

As expected, the model results using with MERIS data were less accurate than those obtained using *in situ* data. The sources of these errors related to field measurement procedures, model assumptions, and atmospheric correction. Field measurements of the above-surface remote sensing reflectance were made several minutes prior to water sampling, leading to a delay between optical and chemical measurements. The model was built using a construction dataset of simulated results of Hydrolight. Although the input parameters of Hydrolight for Chla, NPSS, and CDOM were specific for Lake Taihu, it spatial and temporal differences in IOPs are expected [52]. For example, the Chla specific absorption parameter is expected to vary for species and cell size, in relation to differences in pigment concentrations and packaging effects [52]. In addition, the standard environment parameters used (e.g., solar zenith angle, water depth, and wind speed) did not capture the variability of actual conditions. Variations in the solar zenith angle influence apparent optical properties [48,53]. While the importance of solar zenith angle is less evident in turbid water with respect to Case I waters [54,55], some errors can be associated to the use of these standard parameters. Additional errors associated to the actual wind field and lake topography also occur. Therefore, temporal and geographical differences in real and model IOPs is expected to occur.

The atmospheric correction of MERIS data was another source of error. It would have been possible to check the accuracy of the BEAM atmospheric correction using the field-measured spectra. The above-water reflectance spectra were not measured for the data sets of 24 April, 13 and 16 October 2008 and on 1 May 2011. It was possible to check the BEAM atmospheric correction with *in-situ* measured reflectance spectra measured on 11 June 2007 (Figure 6). This analysis indicated that the mean deviations of reflectance derived from boreal and eutrophic lakes of BEAM ranged from 10% to 90% [44]. We concluded that none of the available MERIS processors provides a good separation of the atmospheric and water-leaving radiance over Lake Taihu.

Figure 6. Comparison of the BEAM atmospheric correction and *in situ* measured reflectance spectra measured on 11 June 2007. The lines represent the reflectance spectra by measurements. The marks represent the atmospheric corrections by BEAM.

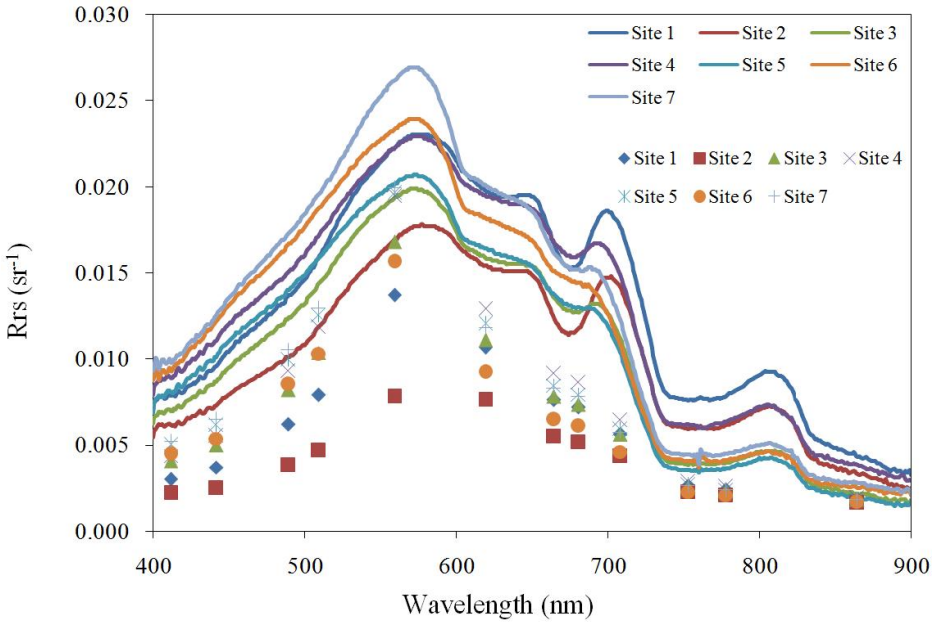

7.2. Application of the Spectral Decomposition Algorithm to Study Chla Spatial Distributions

We applied the new spectral decomposition model to estimate Chla, after having to first remove areas of algal blooms, using Li [14]. The spatial distribution of Chla in the non-bloom areas was determined using four MERIS images (Table 5 and Figure 7). The lake area with Chla less than 30 μg·L^{-1} was 79.14%, 63.92%, 80.04%, and 49.64%, respectively.

In Lake Taihu, the spatial distribution of floating cyanobacteria (e.g., *Microcystis*) is sensitive to wind and lake hydrology [55]. Using the new model in non-bloom areas, Chla was found to be higher in the downwind area, indicating that wind is also an important factor for the Chla distribution in non-bloom areas. At wind speeds below 3.1 m/s, cyanobacteria tend to float to the water surface, favoring the creations of algal blooms [56]. Floating algal blooms were present in the west part of the lake and in Meiliang Bay, a common area for algal blooms [35,57] and may be associated the low average wind speeds measured prior to the measurements; 2.1 and 1.0 m/s on 24 April and 13 October 2008.

Table 5. Coverage percentage of Chla in MERIS images for Lake Taihu.

Range	Time			
	24 April 2008	**13 October 2008**	**16 October 2008**	**1 May 2011**
0 < Chla ≤ 10 μg·L^{-1}	22.27%	9.24%	17.78%	0%
10 < Chla ≤ 20 μg·L^{-1}	26.03%	21.92%	21.13%	16.12%
20 < Chla ≤ 30 μg·L^{-1}	30.84%	32.76%	41.13%	33.52%
30 < Chla ≤ 40 μg·L^{-1}	10.67%	21.47%	14.01%	22.86%
40 < Chla ≤ 50 μg·L^{-1}	7.28%	11.24%	3.18%	12.07%
The rest	2.91%	3.38%	2.77%	15.44%

Figure 7. The estimated distribution of Chla using the spectral decomposition model with MERIS images for 24 April, 13 October and 16 October 2008 and 1 May 2011.

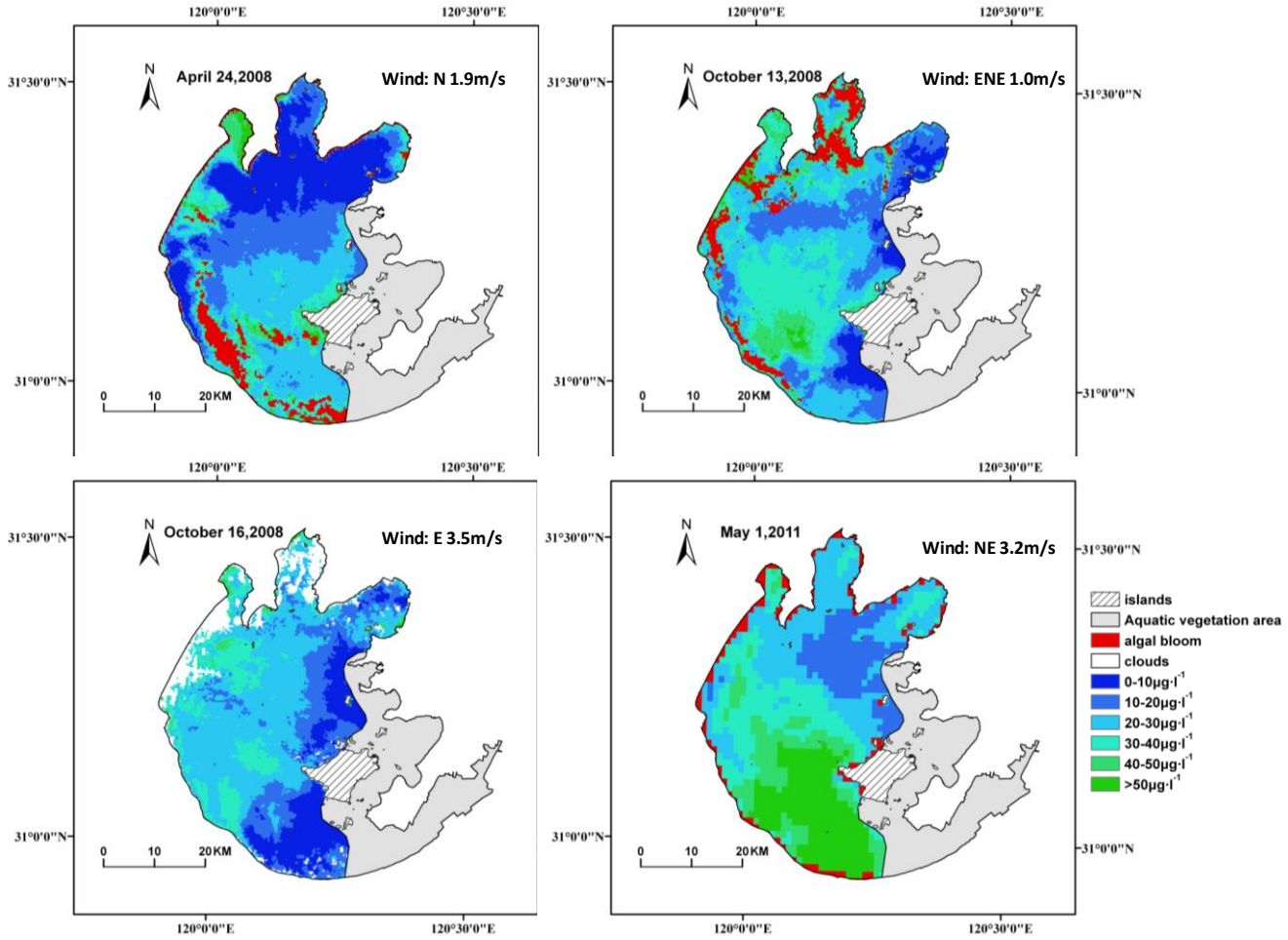

Compared to conventional Chla retrieval models, the spectral decomposition model should be less sensitive to geographic and temporal variability. The spatial distribution of Chla was significantly different in the two images separated by only three days, 13 October and 16 October 2008 (Figure 6). While this is surprising, it is not unusual in Lake Taihu, as the vertical distribution of the dominant cyanobacteria is highly variable and depends on conditions of wind and rain [58].

7.3. The Spectral Decomposition Model Application to Other Satellite Data

If the standard reflectance spectra of the basic components remain consistent and the spectral sensitivity is similar, this model could also be applied with other satellite data. A spectral decomposition model was utilized with Landsat TM data for Chla and NPSS estimates by Oyama [20–22]. Compared with the TM, MERIS provides additional and more appropriate wavebands to estimate Chla [59,60], but this approach is easily transferred to multispectral data from other satellite systems.

8. Conclusions

A novel four end-member spectral decomposition model (including water, phytoplankton biomass, NPSS, and CDOM) was developed to estimate chlorophyll-*a* concentrations in the complex optical

conditions of the eutrophic and shallow Lake Taihu. The validation of the new model indicated that it was appropriate for use with both *in situ* data (*RMSE* = 7.50 $\mu g \cdot L^{-1}$, *RE* = 30.4%) and MERIS data (*RMSE* = 8.45 $\mu g \cdot L^{-1}$, *RE* = 58.6%).

The model was applied to four MERIS datasets for Lake Taihu to estimate chlorophyll-*a* concentrations in areas where surface blooms were not present. The analysis showed that the spatial distribution of chlorophyll-*a* concentrations was strongly influenced by wind conditions, with the higher concentrations in the downwind area. The two spring and two fall analyses indicated that there was an extensive part of the lake with elevated chlorophyll-*a* concentrations, greater than 30 $\mu g \cdot L^{-1}$. These areas ranged between 20% and 50% in these four measurement periods.

The complex optical conditions of many internal waters present challenges to the study of their temporal and spatial dynamics by remote sensing. The spectral decomposition approach developed in the present study is an important new tool to improve our understanding of these aquatic ecosystems. It proved to be more robust estimates using MERIS data than the other eight models explored. Its main limitations are those associated to most models, including errors related to field measurement procedures, radiative transfer model assumptions, and atmospheric correction.

Further research should be performed to explore the use of the spectral decomposition approach to estimate the spatial distribution of the other major optical components, both particulate and dissolved. These developments would require additional research that includes the simultaneous measurement of all major optical components, combining *in situ* and remote data acquisition.

Acknowledgments

We would like to acknowledge the financial supports provided by National High Technology Research and Development Program of China (2014AA06A509), the National Natural Science Foundation of China (No. 41101316, No. 41171271, and No. 41171273), and the 135-Program of NIGLAS (NIGLAS2012135010 and NIGLAS2012135014), and MERIS images provided by the ESA-MOST (China) Dragon 3 Cooperation Programme and Scientific Data Sharing Platform for Lake and Watershed, Nanjing Institute of Geography and Limnology, Chinese Academy of Sciences.

The authors would also like to thank Shan Lin, Wenhua Xiang, Jiawang Rao, Lin Zhou, Linlin Shang, and Guangjia Jiang for their participation in the field experiment.

Author Contributions

Yuchao Zhang had the original idea for the study and with all co-authors carried out the design. Ronghua Ma was responsible for recruitment and follow-up of study participants. Jinduo Xu was responsible for data cleaning. Hongtao Duan and Yuchao Zhang carried out the analyses. Yuchao Zhang drafted the manuscript, which was revised by Steven Loiselle. All authors read and approved the final manuscript.

Conflicts of Interest

The authors declare no conflict of interest.

References

1. Ma, R.H.; Duan, H.T.; Tang, J.W.; Chen, Z.B. *Remote Sensing of Lake Water Environment*; Science Publication: Beijing, China, 2010. (In Chinese)
2. Morel, A.; Prieur, L. Analysis of variations in ocean color. *Limnol. Oceanogr.* **1977**, *22*, 709–722.
3. Gordon, H.R.; Morel, A.Y. Remote Assessment of Ocean Color for Interpretation of Satellite Visible Imagery: A Review. In *Lecture Notes on Coastal and Estuarine Studies*; Springer-Verlag: Berlin, Germany, 1983; p. 114.
4. Sathyendranath, S.; Morel, A. Light emerging from the sea-interpretation and uses in remote sensing. *Remote Sens. Appl. Mar. Sci. Technol.* **1983**, *106*, 323–357.
5. IOCCG. Remote Sensing of Ocean Colour in Coastal, and Other Optically-Complex Waters. In *Reports of the International Ocean-Colour Coordinating Group*; Sathyendranath, S., Ed.; IOCCG: Dartmouth, NS, Canada, 2000; pp. 12–17.
6. Dekker, A.G. Detection of Optical Water Quality Parameters for Eutrophic Waters by High Resolution Remote Sensing. In *Doctorate Thesis in Earth and Life Sciences*; Vrijie Universiteit: Amsterdam, The Netherlands, 1993; pp. 10–13.
7. Gons, H.J. Optical teledetection of chlorophyll-*a* in turbid inland waters. *Environ. Sci. Technol.* **1999**, *33*, 1127–1132.
8. Gitelson, A.A.; Dall'Olmo, G.; Moses, W.M.; Rundquist, D.C.; Barrow, T.; Fisher, T.R.; Gurlin, D.; Holz, J. A simple semi-analytical model for remote estimation of chlorophyll-*a* in turbid waters: Validation. *Remote Sens. Environ.* **2008**, *112*, 3582–3593.
9. Dall'Olmo, G.; Gitelson, A.A. Effect of bio-optical parameter variability on the remote estimation of chlorophyll-*a* concentration in turbid productive waters: Experimental results. *Appl. Opt.* **2005**, *44*, 412–422.
10. Zimba, P.V.; Gitelson, A. Remote estimation of chlorophyll concentration in hyper-eutrophic aquatic systems: Model tuning and accuracy optimization. *Aquaculture* **2006**, *256*, 272–286.
11. Le, C.F.; Li, Y.M.; Zha, Y.; Sun, D.Y.; Huang, C.C.; Lu, H. A four-band semi-analytical model for estimating chlorophyll-*a* in highly turbid lakes: The case of Taihu Lake, China. *Remote Sens. Environ.* **2009**, *113*, 1175–1182.
12. Duan, H.T.; Ma, R.H.; Zhang, Y.Z.; Loiselle, S.A.; Xu, J.P.; Zhao, C.L.; Zhou, L.; Shang, L.L. A new three-band algorithm for estimating chlorophyll concentrations in turbid inland lakes. *Environ. Res. Lett.* **2010**, *5*, 1–6.
13. Yang, W.; Bunki, M.; Chen, J.; Fukushima, T.; Ma, R.H. An enhanced three-band index for estimating Chlorophyll-*a* in turbid Case-II waters: Case studies of Lake Kasumigaura, Japan, and Lake Dianchi, China. *IEEE Geosci. Remote Sens. Lett.* **2010**, *7*, 655–659.
14. Li, Y.M.; Wang, Q.; Wu, C.Q.; Zhao, S.H.; Xu, X.; Wang, Y.F.; Huang, C.C. Estimation of chlorophyll-*a* concentration using NIR/Red bands of MERIS and classification procedure in inland turbid water. *IEEE Trans. Geosci. Remote Sens.* **2012**, *50*, 988–997.
15. Pilorz, S.H.; Davis, C.O. Spectral Decomposition of Sea Surface Reflected Radiance. In Proceedings of the Geoscience and Remote Sensing Symposium, IGARSS '90, 'Remote Sensing Science for the Nineties', 10th Annual International, University of Maryland, College Park, MD, USA, 20–24 May 1990; pp. 345–348.

16. Novo, E.M.; Shimabukuro, Y.E. Spectral mixture analysis of inland tropical waters. *Int. J. Remote Sens.* **1994**, *15*, 1351–1356.
17. Tyler, A.N.; Svab, E.; Preston, T.; Présing, M.; Kovács, W.A. Remote sensing of the water quality of shallow lakes: A mixture modelling approach to quantifying phytoplankton in water characterized by high suspended sediment. *Int. J. Remote Sens.* **2006**, *27*, 1521–1537.
18. Svab, E.; Tyler, A.N.; Preston, T.; Présing, M.; Balogh, K.V. Characterizing the spectral reflectance of algae in lake waters with high suspended sediment concentrations. *Int. J. Remote Sens.* **2005**, *26*, 919–928.
19. Novo, E.M.; Barbosa, C.C.; Freitas, R.M.; Shimabukuro, Y.E.; Melack, J.M.; Filho, W.P. Seasonal changes in chlorophyll distributions in Amazon floodplain lakes derived from MODIS images. *Limnology* **2006**, *7*, 153–161.
20. Oyama, Y.; Matsushita, B.; Fukushima, T.; Naqai, T.; Imai, A. A new algorithm for estimating chlorophyll-*a* concentration from multi-spectral satellite data in case II waters: A simulation based on a controlled laboratory experiment. *Int. J. Remote Sens.* **2007**, *28*, 1437–1453.
21. Oyama, Y.; Matsushita, B.; Fukushima, T.; Matsushige, K.; Imai, A. Application of spectral decomposition algorithm for mapping water quality in a turbid lake (Lake Kasumigaura, Japan) from Landsat TM data. *ISPRS J. Photogramm. Remote Sens.* **2009**, *64*, 73–85.
22. Oyama, Y.; Matsushita, B.; Fukushima, T.; Chen, J.; Naqai, T.; Imai, A. Testing the spectral decomposition algorithm (SDA) for different phytoplankton species by a simulation based on tank experiments. *Int. J. Remote Sens.* **2010**, *31*, 1605–1623.
23. Xiao, C.; Wen, J.G.; Liu, Q.H.; Zhou, Y. Study on spectral unmixing model and its application in extracting chlorophyll concentration of water body. *J. Remote Sens.* **2006**, *10*, 559–567. (In Chinese)
24. Qian, S.; Lin, Q.Z.; Chen, X. An improved method of spectral unmixing of remote sensing image and its application in water pollution monitoring and assessing. *Geogr. Geo-Inf. Sci.* **2003**, *19*, 36–38. (In Chinese)
25. Zheng, Y.F.; Fan, W.H.; Zhang, X.F.; Wu, R.J. Pixel unmixing technology of MODIS remote sensing data. *J. Nanjing Inst. Meteorol.* **2008**, *31*, 145–150. (In Chinese)
26. Lu, C.P.; Lv, H.; Li, Y.M. Algorithms based on spectral decomposition algorithm for retrieval of constituents in Taihu Lake. *J. Geo-Inf. Sci.* **2012**, *13*, 687–694. (In Chinese)
27. Mertes, L.A.K.; Daniel, D.L.; Melack, J.M.; Nelson, B.; Martinelli, L.A.; Forsberg, B.R. Spatial patterns of hydrology, geomorphology, and vegetation on the floodplain of the Amazon River in Brazil from a remote sensing perspective. *Geomorphology* **1995**, *13*, 215–232.
28. Mobley, C.D. *Light and Water: Radiative Transfer in Natural Waters*. Academic Press: New York, NY, USA, 1994.
29. Ma, R.; Jiang, G.; Duan, H.; Bracchini, L.; Loiselle, S.A. Effective upwelling irradiance depths in turbid waters: A spectral analysis of origins and fate. *Opt. Express* **2011**, *19*, 7127–7138.
30. Wang, C.F.; Duan, H.T.; Ma, R.H.; Zhang, Y.C. Inherent optical properties of large lakes in the middle-lower reaches of the Yangtze River: I Absorption. *J. Lake Sci.* **2013**, *25*, 497–504. (In Chinese)
31. Cai, Q.; Gao, X.; Chen, Y.; Ma, S.; Dokulil, M. Dynamic variations of water quality in Lake Taihu and multivariate analysis of its influential factors. *Chin. Geogr. Sci.* **1996**, *6*, 364–374.

32. Chen, Y.W.; Qin, B.Q.; Teubner, K.; Dokulil, M. Long-term dynamics of phytoplankton assemblages: Microcystis- domination in a large shallow lake in China. *J. Plankton Res.* **2003**, *25*, 445–453.
33. Duan, H.; Ma, R.; Zhang, Y.; Loiselle, S.A. Are algal blooms occurring later in Lake Taihu? Climate local effects outcompete mitigation prevention. *J. Plankton Res.* **2014**, *2014*, doi:10.1093/plankt/fbt132.
34. Guo, L. Doing battle with the green monster of Taihu Lake. *Science* **2007**, *317*, doi:10.1126/science.317.5842.1166.
35. Duan, H.T.; Ma, R.H.; Xu, X.F.; Kong, F.X.; Zhang, S.X.; Kong, W.J.; Hao, J.Y.; Shang, L.L. Two-decade reconstruction of algal blooms in China's Lake Taihu. *Environ. Sci. Technol.* **2009**, *43*, 3522–3528.
36. Cai, Y.F. Comparative Study of Composition and Dynamics of Cyanobacteria and Their Driving Factors in Lake Taihu and Lake Chaohu. Ph.D Thesis, Nanjing Institute of Geography and Limnology, Chinese Academy of Sciences, Nanjing, China, 30 May 2009. (In Chinese)
37. Hu, C.H.; Hu, W.P.; Zhang, F.B.; Hu, Z.X.; Li, X.H.; Chen, Y.G. Sediment resuspension in the Lake Taihu, China. *Chin. Sci. Bull.* **2006**, *51*, 731–737.
38. Zhang, Y.L.; Qin, B.Q.; Ma, R.H.; Zhu, G.W.; Zhang, L.; Chen, M.W. Chromophoric dissolved organic matter absorption characteristics with relation to fluorescence in typical macrophyte, algae lake zones of Lake Taihu. *Environ. Sci.* **2005**, *26*, 142–147. (In Chinese)
39. Pope, R.M.; Fry, E.S. Absorption spectrum (380–700 nm) of pure water. II. Integrating cavity measurements. *Appl. Opt.* **1997**, *36*, 8710–8723.
40. Mueller, J.L.; Fargion, G.S.; McClain, C.R. Ocean Optics Protocols for Satellite Ocean Color Sensor. In *Special Topics in Ocean Optics Protocols and Appendices*; Goddard Space Flight Center: Greenbelt, MD, USA, 2003; pp.52–63.
41. Rast, M.; Bezy, J.L.; Bruzzi, S. The ESA medium resolution imaging spectrometer MERIS a review of the instrument and its mission. *Int. J. Remote Sens.* **1999**, *20*, 1681–1702.
42. Gons, H.J.; Auer, M.T.; Effler, S.W. MERIS satellite chlorophyll mapping of oligotrophic and eutrophic waters in the Laurentian Great Lakes. *Remote Sens. Environ.* **2008**, *112*, 4098–4106.
43. Alikas, K.; Reinart, A. Validation of the MERIS products on large European lakes: Peipsi, Vänern and Vättern. *Hydrobiologia* **2008**, *599*, 161–168.
44. Duan, H.T.; Ma, R.H.; Simis, S.G.H.; Zhang, Y.Z. Validation of MERIS case-2 water products in Lake Taihu, China. *GIS Sci. Remote Sens.* **2012**, *49*, 873–894.
45. Earth Observation Toolbox and Development Platform. Available online: http://www.brockmann-consult.de/cms/web/beam (accessed on 26 May 2013).
46. Gitelson, A.; Garbuzov, G.; Szilagyi, F.; Mittenzwey, K-H.; Karnieli, A. Quantitative remote sensing methods for real-time monitoring of inland waters quality. *Int. J. Remote Sens.* **1993**, *14*, 1269–1295.
47. Schalles, J.F.; Gitelson, A.; Yacobi, Y.Z.; Kroenke, A.E. Estimation of chlorophyll from time series measurements of high spectral resolution reflectance in a eutrophic lake. *J. Phycol.* **1998**, *34*, 383–390.
48. Gordon, H. Diffusive reflectance of the ocean: The theory of its augmentation by chlorophyll-*a* fluorescence at 685 nm. *Appl. Opt.* **1979**, *18*, 1161–1166.

49. Moses, W.J.; Gitelson, A.A.; Berdnikov, S.; Povazhnyy, V. Satellite estimation of chlorophyll-*a* concentration using the red and NIR bands of MERIS—The Azov Sea case study. *IEEE Geosci. Remote Sens. Lett.* **2009**, *6*, 845–849.
50. Mishra, S.; Mishra, D.R. Normalized difference chlorophyll index: A novel model for remote estimation of chlorophyll-*a* concentration in turbid productive waters. *Remote Sens. Environ.* **2012**, *117*, 394–406.
51. Zhou, L. Remote Sensing Retrieval of Chlorophyll-*a* Concentration in Lake Waters. Master's Thesis, Nanjing Institute of Geography and Limnology, Chinese Academy of Sciences, Nanjing, China, 30 May 2011. (In Chinese)
52. Sosik, H.M.; Mitchell, B.G. Light absorption by phytoplankton, photosynthetic pigments and detritus in the California current system. *Deep-Sea Res.* **1995**, *42*, 1717–1748.
53. Stramska, M.; Frye, D. Dependence of apparent optical properties on solar altitude: Experimental results based on mooring data collected in the Sargasso Sea. *J. Geogr. Res.* **1997**, *102*, 15679–15691.
54. Kirk, J.T.O. Dependence of relationship between inherent and apparent optical properties of water on solar altitude. *Limnol. Oceanogr.* **1984**, *29*, 350–356.
55. Zhang, M.; Kong, F.; Wu, X.; Xing, P. Different photochemical responses of phytoplankters from the large shallow Taihu Lake of subtropical China in relation to light and mixing. *Hydrobiologia* **2008**, *603*, 267–278.
56. Kong, F.X.; Song, L.R. *Cynobacteria Blooms Formation and Its Environmental Factors*; Science Press: Beijing, China, 2011. (In Chinese)
57. Cao, H.S.; Kong, F.X.; Luo, L.C.; Shi, X.L.; Yang, Z.; Zhang, X.F.; Tao, Y. Effects of wind and wind-induced waves on vertical phytoplankton distribution and surface blooms of microcystis aeruginosa in Lake Taihu. *J. Freshw. Ecol.* **2006**, *21*, 231–238.
58. Huang, Y.P. *Water Environment and Its Pollution Control in Lake Taihu*; Science Press: Beijing, China, 2010. (In Chinese)
59. Odermatt, D.; Vittorio Ernesto Brando, A.G.; Schaepman, M. Review of constituent retrieval in optically deep and complex waters from satellite imagery. *Remote Sens. Environ.* **2012**, *118*, 116–126.
60. Matthews, M.W.; Bernard, S.; Robertson, L. An algorithm for detecting trophic status (chlorophyll-*a*), cyanobacterial-dominance, surface scums and floating vegetation in inland and coastal waters. *Remote Sens. Environ.* **2012**, *124*, 637–652.